PHILOSOPHICAL TRANSACTIONS OF THE ROYAL SOCIETY A MATHEMATICAL, PHYSICAL & ENGINEERING SCIENCES

Electron impact ionization of neutral and ionized fullerenes: ionization cross –sections and kinetic energy release

The Royal Society

Phil. Trans. R. Soc. Lond. A 1999 **357**, 1201-1227
doi: 10.1098/rsta.1999.0371

THE ROYAL SOCIETY

Electron impact ionization of neutral and ionized fullerenes: ionization cross-sections and kinetic energy release

By S. Matt[1], P. Scheier[1], A. Stamatovic[2], H. Deutsch[3], K. Becker[4] and T. D. Märk[1]

[1]*Institut für Ionenphysik, Leopold Franzens Universität, Technikerstr. 25, A-6020 Innsbruck, Austria*
[2]*Faculty of Physics Beograd, PO Box 368, 11001 Beograd, Yugoslavia*
[3]*Institut für Physik, Ernst–Moritz–Arndt Universität, D-17487 Greifswald, Germany*
[4]*Department of Physics and Engineering Physics, Stevens Institute of Technology, Hoboken, NJ 07030, USA*

The unique structure and properties of large carbon clusters, such as C_{60}, made these species the subject of numerous investigations in past years. Here, we will summarize only a small aspect of the diverse research activities involving fullerenes, namely, quantitative knowledge on the formation of positive ions following electron impact on neutral C_{60} and C_{70}. In addition to these electron-impact ionization cross-sections determined for the various ion-formation processes from the neutral targets, which exhibit quite unusual and novel properties, we will also discuss and review recent quantitative results concerning collisions of electrons with mass-selected positive fullerene ions, including excitation and ionization cross-sections, and kinetic energy release distributions.

Keywords: kinetic energy release; partial cross-sections; total cross-sections; ionization of ions; MIKE spectrum; electron-induced dissociation

1. Introduction

Since the first report about the unique structure of C_{60} (and homologous lower and higher fullerenes) by Kroto *et al.* (1985), and the discovery of Krätschmer *et al.* (1990) of how to produce gram quantities of C_{60}, an exciting novel world of chemistry, physics and materials science has developed around this class of molecules and is still growing at a tremendous rate. This unbroken interest is mainly due to the tantalizing properties and fascinating potential applications of this new class of molecules or clusters. In contrast to graphite and diamond, the common forms of carbon, a 'uniquely elegant' structure was suggested for C_{60} by Kroto *et al.* (1985), corresponding to one of the Archimedean semi-regular polyhedra, i.e. a truncated icosahedron with carbon atoms at each of the vertices and σ-bonds along each edge. The resultant soccerball-like structure, consisting of 20 hexagons and 12 pentagons, has been named fullerene and, due to the large empty space inside this cage (with a molecular diameter of *ca.* 7 Å), the bulk density of this new carbon form is only 1.72 g cm^{-3}. Its particular high stability (towards dissociation) is due to (i) its high

symmetry (no weak bonds); (ii) resonance contributions to the stability by the π-like orbitals oriented normally to the surfaces; and (iii) the isolated pentagon rule (Schmalz *et al*. 1988).

Electron interaction with C_{60} or C_{70}, leading to positive or negative ions, exhibits rather unusual and novel properties—unparalleled by other molecular systems. This becomes apparent from a first glance at the corresponding positive or negative mass spectrum. In contrast to 'ordinary' molecules (Märk & Dunn 1985; Illenberger & Momigy 1992) of this size and mass, the parent cation is by far the most abundant ion in the positive mass spectrum, and the negative mass spectrum consists only of the parent anion peak with absolutely no fragment ions present (Lezius *et al*. 1993). As was demonstrated in a number of recent studies about electron ionization and electron attachment of fullerenes, there are many more exciting and novel features not hitherto observed. These include the rather large ionization cross-sections, in particular for the production of anions and multiply charged ions (Lezius *et al*. 1993; Völpel *et al*. 1993; Dünser *et al*. 1995); the possibility of producing highly charged stable fullerene ions (Scheier & Märk 1994; Jin *et al*. 1996); the huge kinetic shifts observed for the production of fragment ions (Foltin *et al*. 1993; Laskin & Lifshitz 1997); and the discovery of novel fragmentation routes of highly excited ions, including autocharge transfer reactions (Scheier *et al*. 1995), sequential decay reactions (Scheier *et al*. 1996*a*), and fission (Dünser *et al*. 1997).

Here, we will summarize only a small aspect of the diverse research activities involving electron collisions with fullerenes, namely the formation of positive ions following electron impact on neutral C_{60} and C_{70}. In addition to these cross-sections for the various ion-formation processes, which exhibit quite unusual and novel properties, we will also discuss quantitative results concerning collisions of electrons with mass-selected positive fullerene ions, including recent cross-section measurements and kinetic energy release distributions. It is interesting to note that electron ionization and electron attachment (see Matt *et al*. (1998*a*) for details), and the discussion of corresponding ion-formation processes, is not only of fundamental interest but in the case of fullerenes, as it turns out, is also of special importance due to possible applications. Because C_{60} can easily accept electrons and form negative ions, it has been suggested as an alternative to SF_6 as an ideal 'broadband' electron scavenger (Scheier & Märk 1997). With alkali metals (e.g. potassium), C_{60} forms a new superconducting crystalline material consisting of a C_{60} ion, with three negative charges, surrounded by three positive potassium ions. This compound becomes superconducting at *ca*. 19 K (Wennerström *et al*. 1996). As the fullerenes can accept and then donate electrons reversibly, the fullerenes may well become catalysts in chemical processes, thus opening a new dimension in chemistry (Schwarz 1993).

2. Experimental techniques

The electron collision measurements with C_{60} were carried out in Innsbruck (Scheier *et al*. 1996*b*), with a double-focusing two-sector field mass spectrometer of reversed Nier–Johnson geometry, with a maximum mass resolution of 25 000 and a mass range of 10 000 amu at a nominal acceleration voltage of 3 kV. Figure 1 shows the experimental set-up schematically. The purified fullerene powder (C_{60}) was evaporated in a special temperature-controlled Knudsen-type oven (with typical temperatures between 800 and 900 K), and introduced as an effusive beam via a small orifice

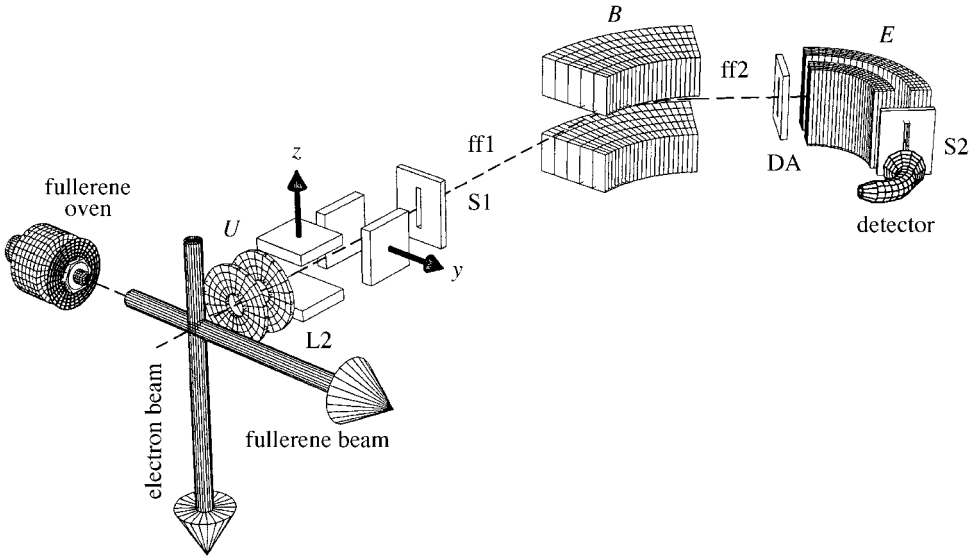

Figure 1. Schematic view of the experimental set-up in Innsbruck after Scheier *et al.* (1996*b*), including a fullerene oven, an electron ion source, and a two-sector field mass spectrometer. S1, Mass spectrometer entrance slit; ff1, first field-free region; ff2, second field-free region; DA, defining aperature; S2, mass-spectrometer exit slit; U, accelerating voltage; B, magnetic field; E, electric field.

and skimmer into the modified Nier-type ion source of the mass spectrometer. After entering the open ion source (with typical background pressures of below 10^{-8} Torr in order to avoid parasitic charge-transfer reactions of the fullerene ions with background molecules), the C_{60} beam (with typical beam flux densities measured with a piezoelectric deposition gauge lying in the range of 10^{14} cm^{-2} s^{-1}), is crossed at right angles by an electron beam. Typical electron currents of approximately 10 μA were used in the case of cross-section measurements, in order to ensure single electron collision conditions, thus limiting the production of highly charged fullerene ions to first-order reactions (Matt *et al.* 1996*a*). The electrons are guided by a weak magnetic field and can have energies varying between approximately 0 and 1000 eV, with an energy spread of approximately 0.5 eV. The ions produced by the two interacting beams are extracted at right angles to the electron and fullerene beam through a slit in the ion source exit electrode by an electric field penetrating from an external electrode L2. For accurate measurements of appearance energies and ionization cross-sections, the ion source exit electrode, the pusher inside the ion source, and the collision chamber housing are kept at the accelerating voltage (typically +3 kV). The extracted ions are focused and steered by additional electrodes, and reach the end of the accelerating region at a grounded earth slit. After entering the mass analyser through the entrance slit, S1, the ions are analysed by the two-sector field instrument and detected by a channeltron, which is connected to a pulse-counting unit and a laboratory computer.

For some of the investigations carried out, it was essential that the two-sector field mass spectrometer allowed the quantitative study of spontaneous or induced dissociations in the two field-free regions of the mass spectrometer. In order to record

the corresponding unimolecular decay peaks in the first field-free region (length: 60.2 cm), the HV-scan technique may be used (Cooks *et al.* 1973). Thereby, the change of the kinetic energy occurring for the ensuing daughter ion is compensated by proper tuning of the acceleration voltage, U. The value, U^*, of the acceleration voltage of the centroid of the metastable peak is related to the mass–charge ratio of the precursor ion and daughter ion, m_1/z_1 and m_2/z_2, respectively, by

$$U^* = U\frac{m_1 z_2}{z_1 m_2}, \tag{2.1}$$

with U the nominal acceleration voltage of the precursor ion. For the investigation of the decay reactions in the second field-free region (length: 33.3 cm), the MIKE scan technique (Cooks *et al.* 1973) is used, which involves the proper tuning of the electric sector field, E. A simple equation, as in the HV-scan, relates the value, E^*, at the centroid of the metastable peak, to the sector field voltage of the precursor ion, E, and the mass–charge ratios of the precursor ion and the daughter ion, i.e.

$$E^* = E\frac{m_2 z_1}{z_2 m_1}. \tag{2.2}$$

Moreover, the MIKE peak shape and, thus, the distance ΔE^* from E^* can be directly related to the kinetic energy release (KER) during the decay reaction. For the decay reaction

$$m_1^{z_1+} \rightarrow m_2^{z_2+} + m_3^{z_3+}. \tag{2.3}$$

The total centre of mass KER can be calculated from ΔE^* of m_2 according to

$$\mathrm{KER} = \frac{m_1^2 z_2^2 eU}{16 m_2 m_3 z_1}\left(\frac{\Delta E^*}{E}\right)^2 = \frac{z_1 eU}{16}\frac{m_2}{m_3}\left(\frac{\Delta E^*}{E_2^*}\right)^2. \tag{2.4}$$

3. Electron ionization cross-sections for C_{60} and C_{70}

Despite many experimental studies about the collisional interaction between electrons and fullerenes (Lifshitz 1993; Scheier *et al.* 1996*b*), so far there exist only a few absolute electron-impact ionization cross-section measurements for C_{60} and C_{70}. This is largely due to the great difficulty in calibrating measured relative cross-section functions, which requires, among other prerequisites, a quantitative knowledge of the neutral fullerene number density in the interaction region of the fullerene gas target and the ionizing electron beam. The only absolute ionization cross-section measurements to date (see also the very recent studies by Foltin *et al.* (1998), Itoh *et al.* (1999) and Tarnovsky *et al.* (1998), mentioned below), are those of Baba *et al.* (1992*a*, *b*), Vostrikov *et al.* (1995), Vostrikov (personal communication), Popovic (personal communication) and, from our laboratory (Dünser *et al.* 1995; Matt *et al.* 1996*a*, 1997*a*). We note that Baba *et al.* (1992*a*, *b*) determined only the C_{60}^+ and C_{70}^+ parent ionization cross-section up to 50 and 80 eV, respectively, using a relative Knudsen-cell approach for the absolute calibration, including a weight-loss experiment that also allows the determination of the fullerene vapour pressure (as discussed recently by Smith (1996) and Gong *et al.* (1996), the vapour thermodynamic properties reported by this group (see Mathews *et al.* 1992) may be in error by as much as a factor of 2.8). Vostrikov *et al.* (1995) determined the total single C_{60} ionization cross-section without mass selection (also using a Knudsen-type technique for the

absolute calibration, relying on the vapour pressure of Mathews *et al.* (1992)). In contrast, we measured a comprehensive set of cross-sections for single and multiple ionization, as well as for dissociative ionization of C_{60} and C_{70}, from threshold to 1000 eV (thereby also allowing determination of the total ionization cross-section) using a novel calibration method (Dünser *et al.* 1995). The absolute cross-section data of Baba *et al.* (1992*a*, *b*) and of Vostrikov *et al.* (1995) are much larger than our corresponding values. In addition, there are significant differences in the energy dependence of the measured cross-section functions.

(*a*) *Partial ionization cross-sections*

For our measurements we used the two-sector field mass spectrometer (described above) invoking, however, for these measurements, a novel technique for the absolute calibration of the cross-sections. The relative partial ionization cross-section functions, for the C_{60} and C_{70} cations, have been obtained following the procedures outlined previously (Grill *et al.* (1993), and references therein) to obtain reliable cross-section data, i.e. using electron currents below 10 μA, and taking into account discrimination effects in the ion source extraction procedure and during the flight through the mass analyser by using the penetration field extraction technique and deflection mass spectrometry technique, respectively. The electron energy scale was calibrated using known cross-section curves for the production of SF_6 anions and the known onsets for partial cross-sections for rare gases. These other gases are introduced into the ion source via supplementary gas inlets. In order to calibrate the measured relative partial ionization cross-sections for the various C_{60-2m}^{z+} and C_{70-2m}^{z+} ions with $m = 0, 1, 2, \ldots$, a novel technique has been employed because the conventional relative flow methods used for ordinary gas targets (Märk & Dunn 1985) cannot be applied here. The key to this new technique lies in the fact that the interaction of electrons with C_{60} (and C_{70}) leads to both negative and positive ions, and that we have recently been able to measure the absolute attachment cross-section function for the production of C_{60}^- using a combination of crossed beams and the flowing afterglow/Langmuir probe technique (Smith *et al.* 1993; Jaffke *et al.* 1994; Matejcik *et al.* 1995). Therefore, measurement of the C_{60}^- and C_{60}^+ ion yield under identical ion source (and mass spectrometer) conditions (gas pressure, electron currents, ion extraction and detection efficiency), should allow us to derive the absolute ionization cross-section for the production of C_{60}^+. As the ion extraction and detection efficiency is, however, usually different for positive and negative ions (in particular in the case of the different electron energies considered), these efficiencies have been determined by Matt *et al.* (1996*a*) using a calibrant gas and corresponding ions, for which both the attachment and the ionization cross-sections are known. Measuring the production of SF_4^+ and SF_4^- via electron interaction, with SF_6 under identical experimental conditions as for the formation of the respective C_{60} ions, the necessary correction factors have been obtained from the ratio of the measured ion currents and the known cross-sections (Margreiter *et al.* 1990; Kline *et al.* 1979). It turns out that the total detection efficiency for the negative ions is approximately a factor of 10 smaller than that for the positive ions, and strongly dependent on the experimental conditions used.

The cross-section thus derived for the production of C_{60}^+ is $(24.6 \pm 8) \times 10^{-20}$ m^2 and for the production of C_{70}^+ it is 19.3×10^{-20} m^2 at an electron energy of 100 eV,

and thus lies way below the other determinations (Baba *et al.* 1992*a*, *b*; Vostrikov *et al.* 1995; Popovic, personal communication) using a Knudsen-cell approach (see below). The error bars given correspond only to the statistical uncertainty and do not include errors in the cross-sections used in the calibration procedure and other systematic errors (see, however, the discussion below). The fact that the C_{70}^{+} parent ion cross-section is smaller than the C_{60}^{+} parent ion cross-section is puzzling at first, because the averaged geometric cross-section (Matt *et al.* 1996*a*) for the ellipsoidal C_{70} is larger than the cross-section of the spherical C_{60}. As will be shown below, the microscopic cross-section to be compared with the geometric cross-section is the counting or the total ionization cross-section rather than the parent cross-sections. Because of the larger contribution from the other partial ionization cross-section channels in the case of C_{70}, the C_{70} counting (or total) ionization cross-section is indeed larger than the corresponding C_{60} cross-section, as expected from simple geometric considerations.

The other partial ionization cross-section functions of C_{60} and C_{70} can then be derived from these parent ion cross-sections determined at an electron energy of 100 eV, and the measured relative partial ionization cross-sections for the other ions. Since this calibration procedure involves a rather complex chain of steps, and relies on previously measured cross-section data as input parameters, we carried out several independent checks on this calibration procedure, all of them confirming the results obtained (see Matt *et al.* (1996*a*, *b*) for details). This is the first time that this calibration procedure has been used, but it has obvious value for the quantitative study of electron-impact ionization of other normally solid substances, such as polycyclic aromatic hydrocarbons, a topic of current interest in mass spectrometry and astrochemistry.

So far we have determined the following partial ionization cross-section curves (Dünser *et al.* 1995; Matt *et al.* 1996*a*, 1997*a*), including 22 partial cross-sections for C_{60}, C_{60}^{k+} ($k = 1$–4), C_{58}^{l+}, C_{56}^{l+}, C_{54}^{l+}, C_{52}^{l+} ($l = 1$–3), C_{50}^{m+}, C_{48}^{m+} ($m = 1, 2$), C_{46}^{+}, C_{44}^{+}, and 34 partial cross-sections for the heavier fullerene C_{70}, C_{70}^{j+} ($j = 1$–6), C_{68}^{k+}, C_{66}^{k+} ($k = 1$–4), C_{64}^{l+}, C_{60}^{l+} ($l = 1$–4), C_{62}^{m+}, C_{58}^{m+} ($m = 1$–3), C_{56}^{n+}, C_{54}^{n+} ($n = 2, 3$), C_{52}^{2+}, C_{50}^{2+}. For both C_{60} and C_{70}, ion signals from smaller fragment ions, as well as from more highly charged ions, were recorded, but generally complete ionization cross-section curves were only measured when the maximum cross-section was larger than 0.1% of the maximum value of, respectively, the C_{60}^{+} and C_{70}^{+} single parent ionization cross-sections (0.1% cut-off). Figure 2 displays the maximum cross-section values on a logarithmic scale, plotted against the cluster size for C_{60} and C_{70}, respectively. Figures 3 and 4 show, as an example, some of the C_{60} and C_{70} cross-section curves.

A close inspection of these fullerene ionization cross-section data reveals many surprising features that distinguish the fullerenes C_{60} and C_{70} from other complex polyatomic molecules (Märk & Dunn 1985; Märk 1984). Experience has shown that single ionization is by far the most dominant channel for almost all polyatomic molecules. Cross-sections for the formation of doubly charged ions are typically about two orders of magnitude smaller than single ionization cross-sections, and cross-sections for the formation of more highly charged ions are usually negligible. Furthermore, dissociative ionization becomes increasingly important for more complex target molecules and, in many cases, fragment ions are formed with cross-sections that are significantly larger than the parent ionization cross-section. The following general observations regarding the various partial ionization cross-sections for C_{60} and C_{70} are noteworthy.

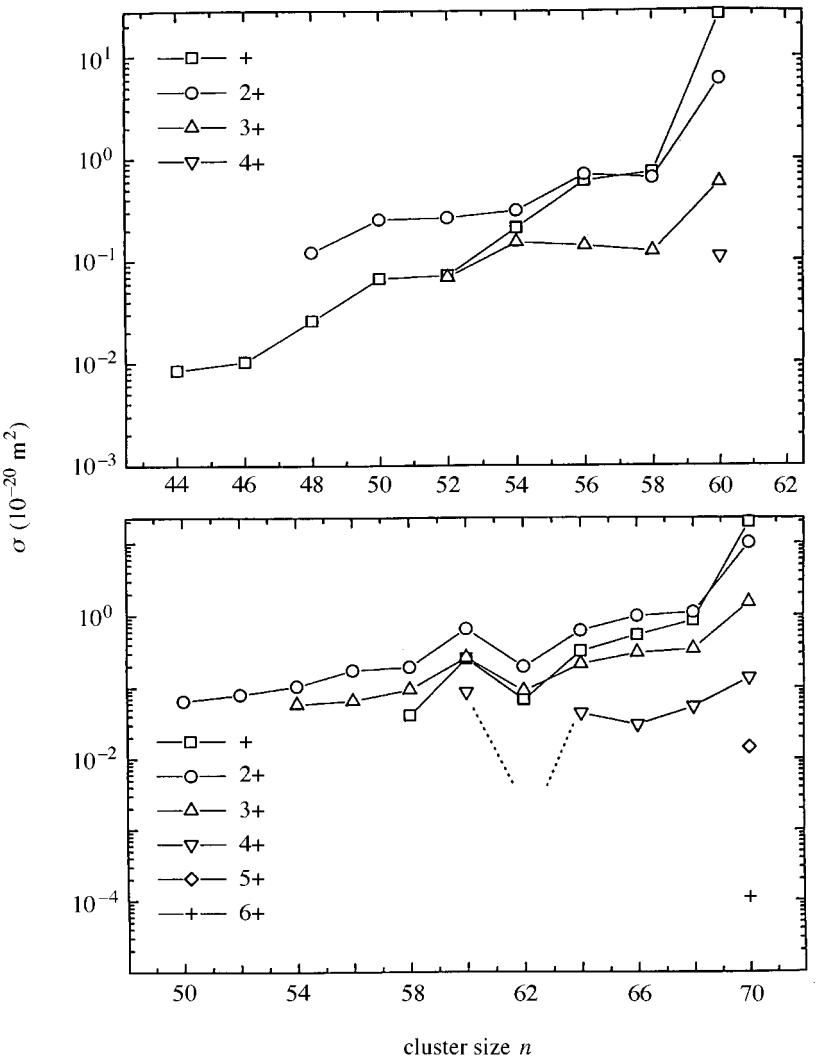

Figure 2. Maximum partial electron ionization cross-sections for (*a*) singly, doubly, triply and quadruply charged parent and fragment ions of C_{60} and (*b*) singly, doubly, triply, quadruply, quintuply and sextuply charged parent and fragment ions of C_{70} (after Matt *et al*. 1996*a*, 1997*a*).

(1) The formation of the *singly charged parent* ion C_{60}^+, or C_{70}^+, has the largest cross-section. Although this is in contrast to the situation known for ordinary larger polyatomic molecules (where the parent ion is usually almost non-existent, with the exception of the case of some polycyclic aromatic hydrocarbons). It is nevertheless in accordance with previous mass-spectrometric studies and theoretical considerations (RRKM calculations) of the ionization and fragmentation of C_{60} (Foltin *et al*. 1993; Lifshitz 1993). The large binding energy, and the large number of degrees of freedom (and the resulting huge kinetic shift of more than 34 eV), render dissociative ionization processes of C_{60} less likely (according to these measurements approximately a factor of 20 or less). In addition,

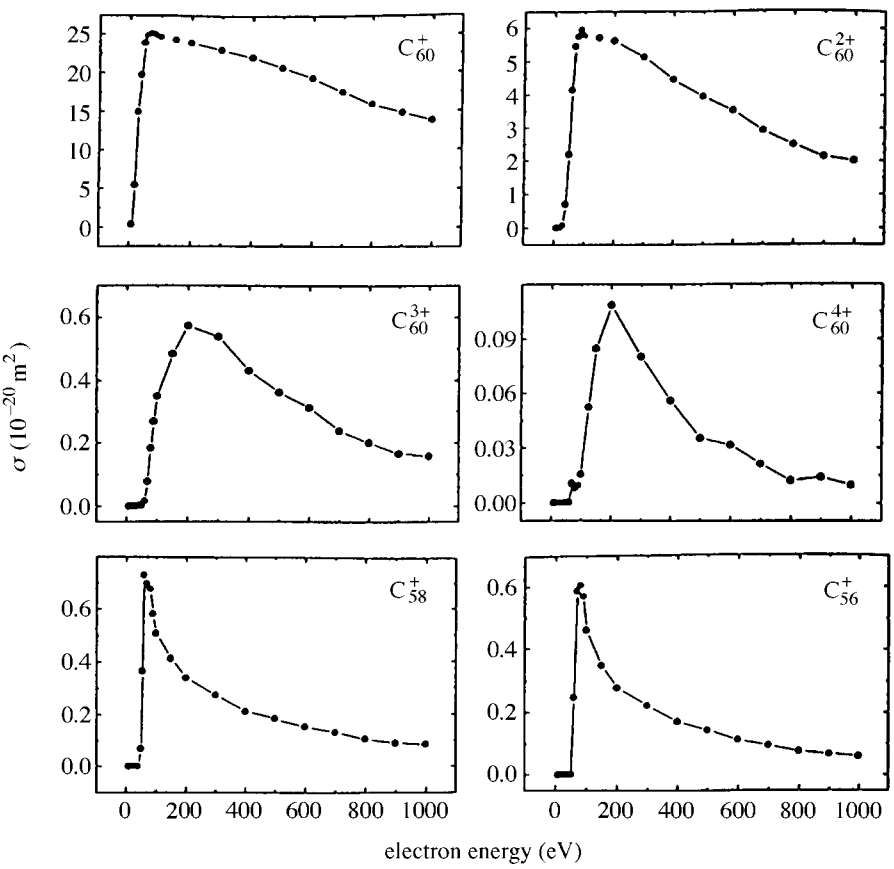

Figure 3. Absolute partial electron ionization cross-sections versus electron energy for the formation of singly, doubly, triply and quadruply charged C_{60} parent ions and for the formation of singly, doubly and triply charged C_{58} and C_{56} fragment ions from C_{60} (after Matt *et al*. 1996*a*).

these facts are also responsible for the very large appearance energies observed (Wörgötter *et al*. 1994; Matt *et al*. 1997*a*) for fullerene fragment ions (more than *ca*. 45 eV). It is also interesting to note that the maximum value for the process $C_{60} + e \rightarrow C_{60}^{+}$ of $25 \times 10^{-20}\,m^2$ is just slightly larger than the value of $21 \times 10^{-20}\,m^2$ reported previously by Völpel *et al*. (1993) for the electron-impact ionization of $C_{60}^{+} + e \rightarrow C_{60}^{2+}$. This is not surprising, taking into account that the highest occupied molecular orbital level, h_u, of the neutral molecule is tenfold degenerate (Yannouleas & Landman 1994), and that the removal of the first two π-electrons requires rather similar ionization energies of 7.6 and 11.4 eV, respectively.

(2) *Multiply charged parent ions* are formed with significant cross-sections, e.g. the maximum cross-section for the formation of C_{60}^{2+} and C_{70}^{2+} amounts to about half of the maximum of the respective singly charged parent cross-section. Even the triply charged parent ion is formed with a cross-section that exceeds the cross-section for the formation of any fragment ion. It is interesting to note that this feature of the fullerenes is quite different from the behaviour observed for

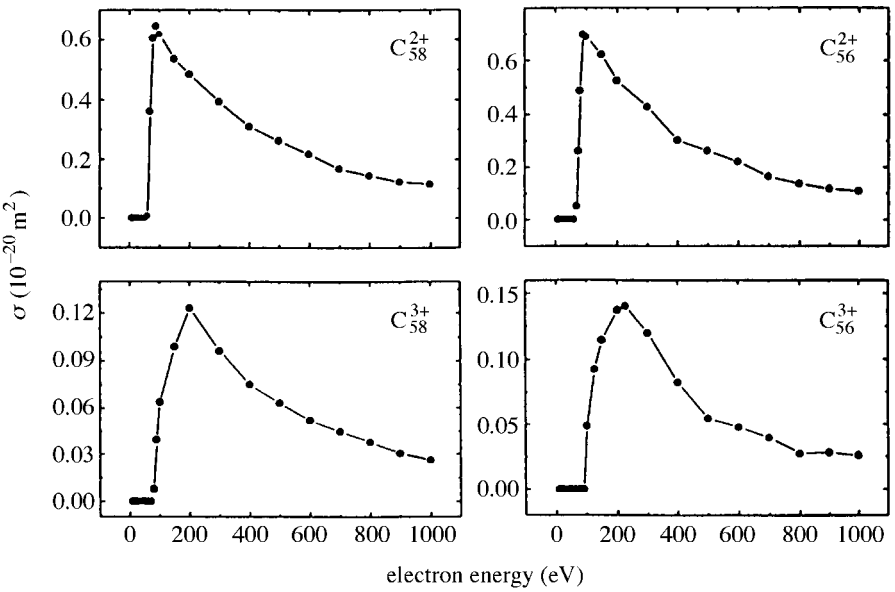

Figure 3. (*Cont.*)

ordinary molecules and atoms, as the ratio between doubly and singly charged ions is seldom more than a few per cent (i.e. the gas with the highest percentage of doubly charged ions known so far is Xe, with approximately 11% (see Märk 1984)). The reason for this enhanced production of doubly and higher-charged ions lies, on the one hand, in the fact that the production of doubly and triply charged ions is energetically more favourable than the production of fragment ions (Wörgötter *et al.* 1994; Matt *et al.* 1997*a*), and, on the other hand, that due to the spheroidal shape of C_{60}, and the ellipsoidal shape of C_{70}, secondary electrons from an initial single ionization reaction may be ejected into the empty space inside the fullerene cage, and, subsequently, interact again with the electron shell of the quantum system, thus drastically enhancing the chance for the occurrence of inelastic multiple electron collisions. Similar effects have been observed for the production of multiply charged cluster ions (see the recent review by Echt & Märk (1994) for details).

(3) For all of the *fullerene fragment ions*, the formation of the doubly charged fragment ion has a larger cross-section than the formation of the respective singly charged fragment ion. The amount by which the double ionization cross-section exceeds the single ionization cross-section increases, for instance, for the larger fullerene C_{70} systematically with decreasing fragment-ion size from 40% for C_{68} to a factor of five for C_{58} ions. Furthermore, for C_{62}, C_{60} and C_{58}, even the triple-ionization cross-section exceeds the respective single-ionization cross-section.

(4) For all fragment ions, multiple ionization is more prominent than dissociative ionization, i.e. $\sigma_{\max}(C_{2n}^{2+}) > \sigma_{\max}(C_{2n-2}^{+})$.

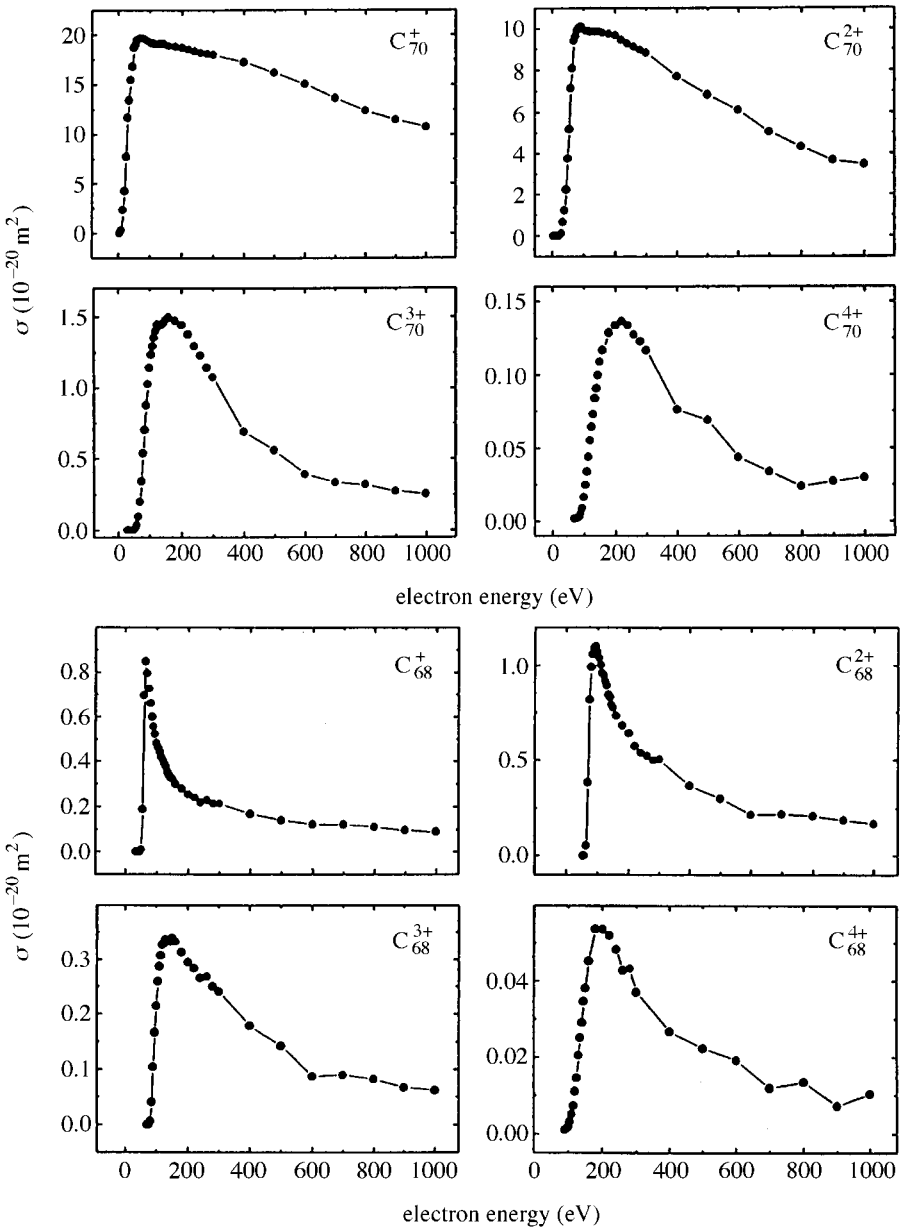

Figure 4. Absolute partial electron ionization cross-sections versus electron energy for the formation of singly, doubly, triply and quadruply charged C_{70} parent ions and for the formation of singly, doubly, triply and quadruply charged C_{68} fragment ions from C_{70} (after Matt *et al.* 1996*a*).

These general findings are qualitatively true for C_{60} and C_{70}, with only a few minor exceptions, such as the fact that the doubly charged parent ion, C_{60}^{2+}, is formed with a cross-section of only $\frac{1}{3}$ of the C_{60}^{+} cross-section (as compared with a factor of $\frac{1}{2}$ for C_{70}). The main difference between C_{60} and C_{70} is the fact that more fragment

ions, and more highly charged parent and fragment ions, are formed with appreciable cross-sections from C_{70}. The larger number of partial C_{70} ionization cross-sections of appreciable magnitude, compared to C_{60}, results in a total C_{70} ionization cross-section that is larger than the total C_{60} ionization cross-section, even though the single parent C_{60}^+ cross-section is larger than the corresponding C_{70}^+ cross-section. Moreover, we note that the formation of the singly and multiply charged C_{60} partial ionization cross-sections from C_{70} exhibit a significant increase compared to the corresponding cross-sections for the adjacent C_{62} and C_{58} fragments (see figure 2). This can be explained in terms of the highly ordered geometry of the C_{60} cluster, as a magic number effect.

In addition to the above findings regarding the ordering of the maximum values of the partial ionization cross-sections (see figure 2), a close inspection of the shape of the cross-section curves reveals several additional interesting features, which can be summarized as follows.

(1) There appears to be a systematic change in the ionization curves for the *parent ion* with increasing charge state. The C_{60}^+ and the C_{70}^+ parent ionization cross-section curves have an unusually broad maximum (as compared to cross-section curves known for other molecules), followed by a very gradual decline towards higher electron energies. As the charge state increases, the maximum becomes narrower and more sharply peaked, i.e. the cross-section curves decline more rapidly between the position of the maximum and *ca.* 500 eV. Above 500 eV, these cross-section curves exhibit a rather flat energy dependence.

(2) All *fragment ions* show essentially similar cross-section shapes, which are very different from the parent ionization cross-section functions. The singly charged fragment-ion formation is characterized by a rapidly rising cross-section from threshold with a pronounced maximum at comparatively low impact energies, followed by a steep decline to *ca.* 200 eV. Above 200 eV, the cross-section functions of all singly charged fragment ions are essentially flat. As the charge state of the fragment ion increases, the maximum in the cross-section function becomes gradually broader, and the cross-section declines more gradually towards higher impact energies. Above *ca.* 500 eV, all fragment multiple-ionization cross-sections are essentially flat.

(*b*) *Time-integrated partial ionization cross-section*

Finally, we would like to mention that the cross-sections reported by Matt *et al.* (1996*a*) correspond to the electron-impact induced production of stable parent and fragment ions, i.e. of ions produced and extracted from the ion source that survive the total flight through the mass analyser system without spontaneous (metastable) decay. Ions that decay by metastable dissociations will be lost in the experimental set-up (as they are leaving the phase space settings of the considered ion in the mass-spectrometer system), and therefore will not be accounted for in these measurements. Some of the fragment ions of C_{60} and C_{70} (and even the parent ions) exhibit, however, rather strong metastable fragmentation reactions on their way from the ion source, through the mass analyser, to the detector. In order to obtain accurate ('true') ionization cross-sections for a specific ion under study, it is necessary to add to the measured ion current for this particular ion, the ion currents of all possible fragment

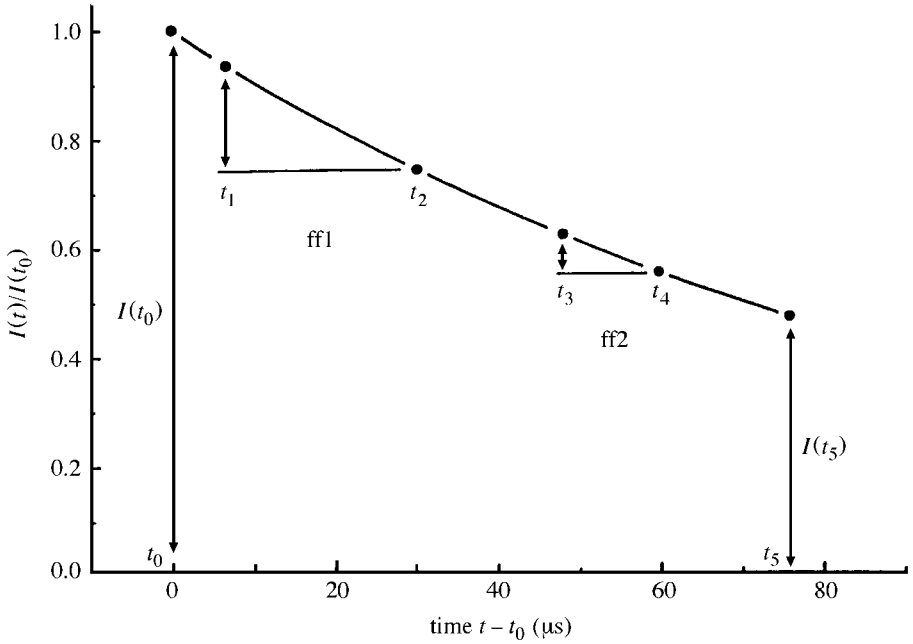

Figure 5. Schematic diagram of the time-scale involved in the experiment shown in figure 1. The time t_0 refers to the time at which the ions leave the ion source of the mass spectrometer. The time-intervals marked respectively by t_1 and t_2, and by t_3 and t_4 designate the flight time of the ions through the first (ff1) and second (ff2) field-free region, and the time t_5 marks the arrival of the ions at the detector (see text).

ions produced from this particular ion during its flight through the mass analyser. The ion currents I_{2n} of C_{2n}^{z+} ions measured in our earlier experiment (Matt *et al.* 1996*a*) result from those ions formed in the ion source (i.e. within a time t_0 after ionization), that survive the flight time through the mass spectrometer and arrive at the detector at a time t_5 after ionization without further fragmentation (see figure 5). The major decay reaction for fullerene ions (see Scheier *et al.* (1996*a*, *b*) and Dünser *et al.* (1997) for details), i.e.

$$C_{2n}^{z+} \rightarrow C_{2n-2}^{z+} + C_2, \tag{3.1}$$

results in a measured ion current $I_{2n}(t_5)$, which is less than $I_{2n}(t_0)$. In a two-sector field mass spectrometer, like the one shown in figure 1, it is not possible to directly determine the loss of C_{2n}^{z+} ions on the way from the ion source to the detector, since we cannot measure fragment-ion currents in the magnetic and electric sector field regions. However, by decoupling the magnetic and the electric sector field (see above), it is possible to measure these currents in the two field-free regions of the mass spectrometer, i.e. the fragment-ion current $I_{\mathrm{ff1}} = I_{2n}(t_1) - I_{2n}(t_2)$, from ions formed in the time interval between t_1 and t_2 in the first field-free region (ff1), and the fragment-ion current $I_{\mathrm{ff2}} = I_{2n}(t_3) - I_{2n}(t_4)$ from ions formed in the time interval between t_3 and t_4 in the second field-free region (ff2). We will discuss, in the following, how one can use the measured (Scheier *et al.* 1996*a*; Foltin *et al.* 1997) fractions $\mathrm{MF}_{2n}(\mathrm{ff1}) = I_{\mathrm{ff1}}/I_{2n}(t_5)$, and $\mathrm{MF}_{2n}(\mathrm{ff2}) = I_{\mathrm{ff2}}/I_{2n}(t_5)$ to extrapolate the

measured ion currents $I_{2n}(t_5)$ to time t_0 using the 'evaporative ensemble theory' (EET) of Klots (1985, 1990). For more details see Foltin *et al.* (1998).

If one assumes that a C_{2n}^{z+} ion is formed by fragmentation of the precursor C_{2n+2}^{z+} ion in the ion source, and that it further fragments via reaction (3.1) on the way to the detector, the EET expresses the ratio $I_{2n}(t)/I_{2n}(t_0)$ in the form of an integral of many single-exponential decay terms, which cover a range of internal energies of C_{2n}^{z+} from E_1 to E_2. The energy E_1 is related to the energy needed to produce C_{2n}^{z+} from C_{2n+2}^{z+} within a time t_0, and E_2 is the energy required to further fragment C_{2n}^{z+} within a time t_0. One finds that the ratio $P(t) = I_{2n}(t)/I_{2n}(t_0)$ is largely independent of the nature of the ionization process and of the electron energy E_e. Under some additional assumptions, which can be justified for larger clusters, the ratio $P(t)$ can be expressed in a simple form as a function of three thermodynamical parameters (i.e. the heat capacity C, the so-called Gspann parameter γ, and the ratio of dissociation energies of C_{2n}^{z+} and C_{2n+2}^{z+}, $\Delta E_a(2n)/\Delta E_a(2n+2)$), and the time t_0:

$$\left.\begin{aligned} P(t) &= \frac{C^*}{Y^{*2}} \ln\left[1 + \left(\exp\left(\frac{\gamma^{*2}}{C^*}\right) - 1\right)\frac{t_0}{t}\right], \\ \gamma^* &= \gamma\sqrt{1 + \left(\frac{C}{\gamma}\left(1 + \frac{\gamma}{2C} + \frac{\gamma^2}{12C^2} + \cdots\right) - 1\right)\frac{\Delta E_a(C_{58}^+) - \Delta E_a(C_{60}^+)}{\Delta E_a(C_{58}^+)}}, \\ C^* &= C\left(1 - \frac{\gamma}{2C} + \frac{\gamma^2}{12C^2} + \cdots\right)^2. \end{aligned}\right\} \tag{3.2}$$

The heat capacity can be calculated easily and the ratios of the dissociation energies may be taken from Matt *et al.* (1997*b*) and Wörgötter *et al.* (1996). In order to obtain the Gspann parameter $\gamma = \Delta E_a(2n)/k_B T$, equation (3.2) is fitted separately to the measured metastable fractions $MF_{2n}(ff1)$ and $MF_{2n}(ff2)$. The correction factors $I_{2n}(t_0)/I_{2n}(t_5)$ obtained, averaged for the two field-free regions, are 1.025, 1.091 and 1.187 for singly, doubly and triply charged C_{60} ions (using an even simpler form than equation (3.2) (see Foltin *et al.* 1998)), and 1.532, 1.920 and 1.966 for the respective C_{58} ions. For C_{2n}^{z+} ions with $2n < 58$, the metastable fractions $MF_{2n}(ff2)$ and $MF_{2n}(ff1)$ cannot be measured with sufficient accuracy. However, the heat capacity C will be very similar for C_{56}^+ and C_{58}^+ ions, as will be the Gspann parameter, γ, and the ratio of the dissociation energies $\Delta E_a(2n)/\Delta E_a(2n+2)$. As a consequence, formula (3.2) implies that $I_{56}(t_0)/I_{56}(t_5) \approx I_{58}(t_0)/I_{58}(t_5)$ and, therefore, it is justifiable to use the same factor $I_{58}(t_0)/I_{58}(t_5)$ to correct the ionization cross-sections for C_{2n}^{z+} ions with $2n < 58$. This yields somewhat less accurate results for $2n < 58$. However, the C_{2n}^{z+} ions with $2n < 58$ contribute less to the total ionization cross-sections and, hence, this approximation will not introduce a significant error in the total ionization cross-sections for C_{60}. Two trends are apparent from the correction factors obtained. The correction factors are larger for the decay of fragment ions (e.g. C_{58}^{z+}) than for the decay of the C_{60}^{z+} parent ions and for a given fragment ion, the correction factors increase with the charge of the precursor ion, i.e. the correction increases from C_{2n}^+ to C_{2n}^{2+} to C_{2n}^{3+}. The overall smallest correction of *ca.* 2.5% applies for the C_{60}^+ parent ion.

The ratios $I_{2n}(t_0)/I_{2n}(t_5)$ obtained from the above described procedure can be used to extrapolate the measured ion currents $I(t_5)$ to time t_0 and thus, to account

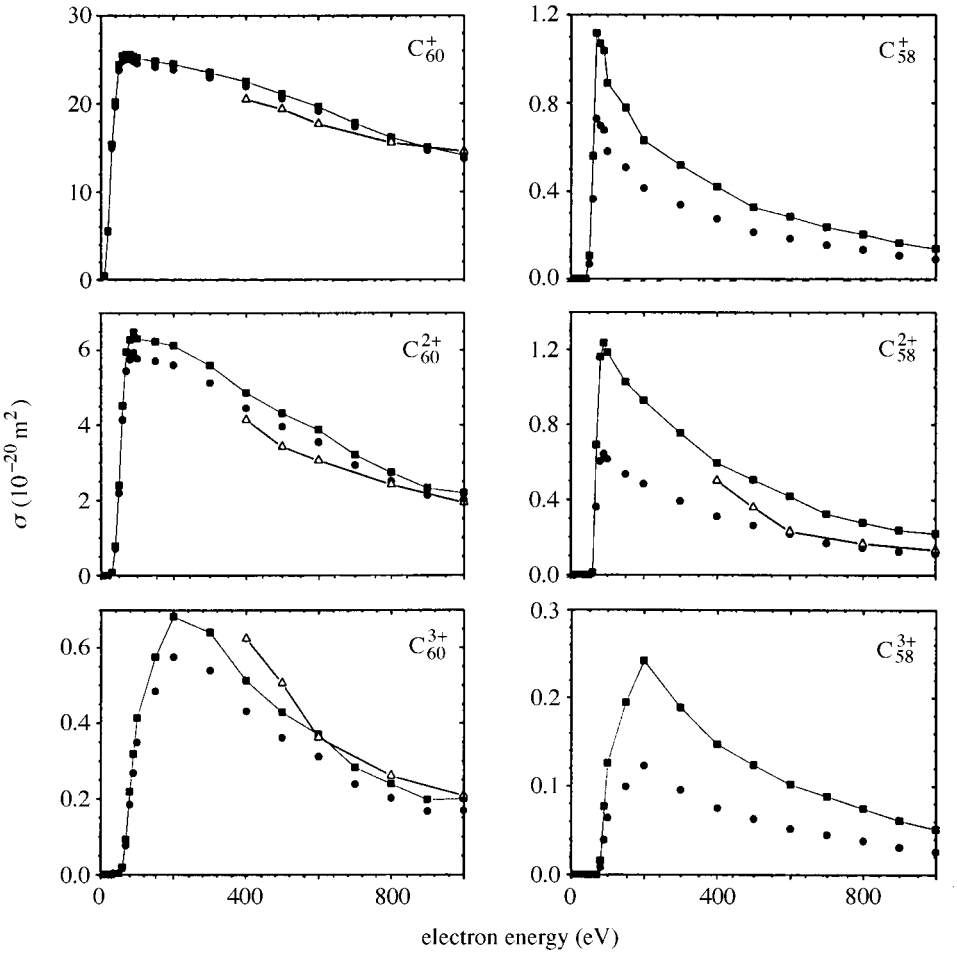

Figure 6. Absolute partial electron ionization cross-sections versus electron energy up to 1000 eV for the formation of singly, doubly and triply charged C_{60} parent ions (left column from top to bottom) and for the formation of singly, doubly and triply charged C_{58} fragment ions from C_{60} (right column from top to bottom); after Matt *et al.* (1996*a*), designated by full dots, and after Foltin *et al.* (1998), designated by full squares connected by a line to guide the eye. Also shown for comparison are recent data by Itoh *et al.* (1999) designated by open triangles.

for the ion currents that were lost in the previous experiment by Matt *et al.* (1996*a*) due to fragmentation processes. This, in turn, allows one to correct the previously reported absolute cross-section functions. Figure 6 compares the previously reported (full dots) and corrected (full squares connected by a line to guide the eye) ionization cross-section values for a few selected partial cross-sections. This figure shows how the correction increases with the charge state of the precursor ion for C_{60}^{z+}, $z = 1$–3 (left column) and C_{58}^{z+}, $z = 1$–3 (right column). A comparison of the two columns also shows that, overall, the corrections are much larger for the C_{58}^{z+} fragment ions than for the C_{60}^{z+} parent ions.

Very recently, two additional absolute cross-section measurements have been carried out (in both cases without experimental complication, due to the decaying

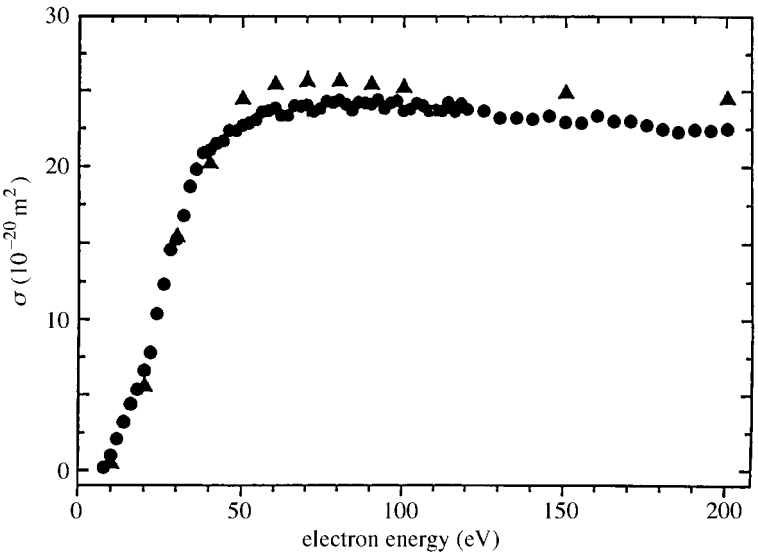

Figure 7. Absolute partial electron ionization cross-sections versus electron energy from threshold up to 200 eV for the formation of singly charged C_{60} parent ions, after Matt *et al.* (1996*a*) and corrected by Foltin *et al.* (1998) (designated by full dots) and after Tarnovsky *et al.* (1998) (designated by full triangles).

metastable ions) and the results obtained are included in figures 6 and 7. Itoh *et al.* (1999), using a time-of-flight mass spectrometer, measured the partial cross-sections for the production of the parent ions C_{60}^{z+}, $z = 1$–3, and calibrated the relative cross-sections by using the vapour pressure data reported by Abrefah *et al.* (1992) (for the reliability of this vapour pressure, see the discussion in Smith (1996) and Gong *et al.* (1996)). Due to the low sensitivity of their apparatus, Itoh *et al.* (1999) were able to measure the cross-sections for only two of the many fragment ions, i.e. C_{58}^{2+} and C_{56}^{2+} (the cross-section for the these two ions was found to be about the same). The agreement between the corrected cross-sections of Matt *et al.* (1996*a*) (using the method of Foltin *et al.* (1998)), and those of Itoh *et al.* (1999), is excellent in the overlapping energy range between 400 and 1000 eV (see figure 6). Moreover, Tarnovsky *et al.* (1998) carried out a very careful study on the absolute cross-section for the production of C_{60}^{+} using the reliable fast-neutral-beam technique (Tarnovsky & Becker 1993), which allows the absolute calibration of ionization cross-sections without the need to normalize the relative cross-section to a previously determined benchmark cross-section. In particular, the fast-neutral-beam technique avoids (as does the method used by Matt *et al.* (1996*a*)) the problems associated with the direct determination of the fullerene pressure in the ion source (i.e. the use of unreliable vapour pressure data (see Smith 1996; Gong *et al.* 1996)) by determining the neutral gas density from a measurement of the energy deposited by the fast neutral target beam into a calibrated pyroelectric detector. As can be seen in figure 7, the agreement between the two independent cross-section measurements of Tarnovsky *et al.* (1998) and Matt *et al.* (1996*a*) is excellent over the entire overlapping energy range from the onset up to 200 eV.

Two interesting conclusions can be drawn from this excellent agreement between these three data-sets shown in figures 6 and 7. First, the close agreement between

these three independent measurements and thus, the large discrepancy of these three data-sets with the results of Baba *et al.* (1992*a*, *b*), Vostrikov *et al.* (1995) and Popovic (personal communication), which exhibit much larger cross-sections and quite different cross-section shapes, strongly suggests that the data of Baba *et al.* (1992*a*, *b*), Vostrikov *et al.* (1995) and Popovic (personal communication), suffered by the unreliable vapour pressure data used for calibration, and in addition by discrimination effects leading to artifacts in the measured cross-section curves. Second, the excellent agreement of the corrected data of Matt *et al.* (1996*a*), with those of Tarnovsky *et al.* (1998) and Itoh *et al.* (1999), serves as an independent confirmation of the reliability of the C_{60}^- attachment cross-section used in the absolute calibration by Matt *et al.* (1996*a*) (see above). This is important as the uncertainty in the C_{60}^- attachment cross-section represented the largest contribution to the total uncertainty of the cross-sections reported by Matt *et al.* (1996*a*), as discussed in detail by Matt *et al.* (1998*a*).

(*c*) *Total ionization cross-sections*

Adding the various measured partial ionization cross-sections for C_{60} and C_{70} gives the corresponding total ionization cross-sections (weighted sum) and the total counting cross-sections (simple sum). It is interesting to note (see figure 8, showing the uncorrected data of Matt *et al.* (1996*a*)), that the maximum total ionization cross-section and the maximum counting ionization cross-section of C_{70} exceeds the corresponding C_{60} ionization cross-section by *ca.* 20.7% and 5%, respectively, even though the dominant single C_{60}^+ parent ionization cross-section was found to exceed the corresponding single C_{70}^+ parent cross-section by 21.5%. The reverse ordering of the total ionization cross-section, and the counting ionization cross-sections, reflects the fact that there exist, for C_{70}, more fragment ionization cross-sections and more cross-sections for the formation of multiply charged ions of appreciable magnitude (above the 0.1% cut-off) than for C_{60}. Moreover, figure 9 compares the previously reported (Matt *et al.* 1996*a*) and the corrected (Foltin *et al.* 1998) ionization cross-section values for the total C_{60} ionization cross-section (bottom diagram, σ_{total}), the total C_{60} counting cross-section (centre diagram, σ_{counting}), and the total cross-section for the formation of singly charged C_{60} ions (top diagram, σ_{total}^+). As expected on the basis of the correction factors mentioned above, the largest correction, an increase of 16.6%, has to be applied to the total cross-section, whereas the correction applied to the counting cross-section amounts to only 11.7%. The total cross-section for the formation of singly charged C_{60} ions is least sensitive to metastable ion losses, and the correction factor here is less than 5.6%. This can be understood on the basis of the fact that (i) the C_{60}^+ ionization cross-section is least sensitive to metastable decay losses with a correction of only *ca.* 2.5% combined with (ii) this cross-section is by far the largest C_{60} partial ionization cross-section.

The experimentally determined molecular ionization cross-section, most readily compared with calculated cross-sections, is usually the total single ionization cross-section. However, the data of Matt *et al.* (1996*a*) indicate that the total single ionization cross-section for C_{60} is essentially identical to the single parent ionization cross-section, since the sum of all dissociative ionization cross-sections of C_{60} has a maximum value of less than *ca.* 5% of the single C_{60}^+ parent ionization cross-sections. Moreover, it has been argued by Matt *et al.* (1996*a*) on the basis of the cage structure

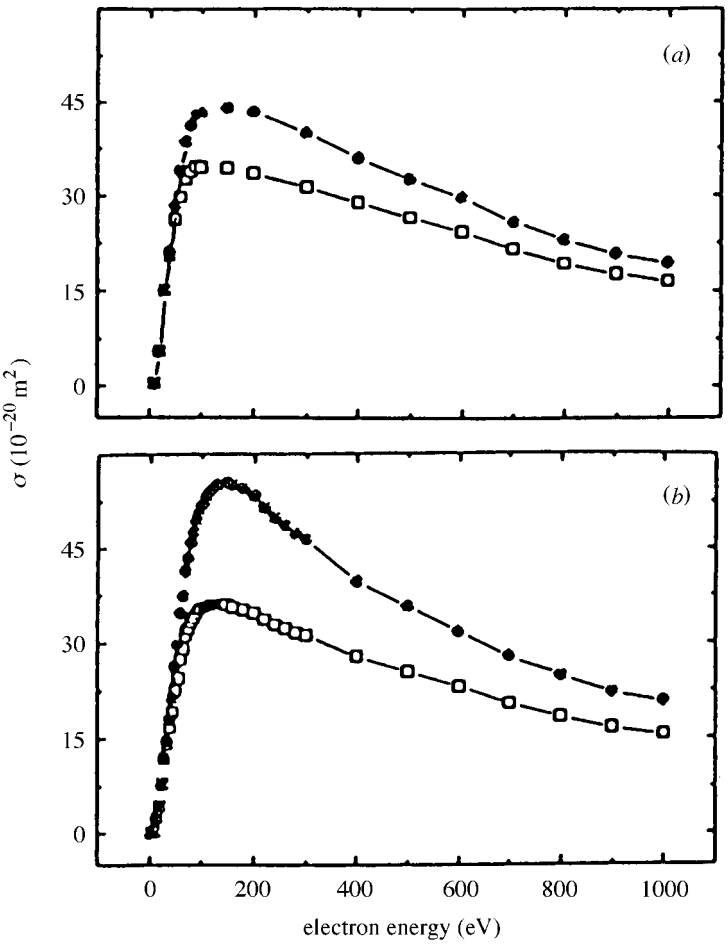

Figure 8. Absolute counting (designated by open squares) and total (designated by solid circles) electron ionization cross-section curves for C_{60} (*a*) and C_{70} (*b*) after Matt *et al.* (1996*a*). For corrected values see figure 9.

of C_{60} that it would perhaps be more appropriate to compare the measured counting cross-section with the calculated ionization cross-section. Alternatively, one might think of the measured total single ionization cross-section as a lower bound of the calculated cross-section and consider the counting cross-section an upper bound in the case of C_{60}. Thus, in figure 10, we compare the corrected $\sigma^{+}_{\mathrm{total}}$ cross-section (curve 4) and the total counting cross-section $\sigma_{\mathrm{counting}}$ (curve 5) of Matt *et al.* (1996*a*) with the experimental cross-sections of Baba *et al.* (1992*a*, *b*) and Vostrikov *et al.* (1995). Also shown are the results of two calculations using (i) the semi-empirical DM formalism of Deutsch *et al.* (1996) (curve 1); and (ii) a recently introduced modified additivity concept (curve 6). Both calculations appear to overestimate the corrected data of Matt *et al.* (1996*a*) (curve 4). Conceptually, the DM calculation relies on the additivity rule, which builds the total single ionization cross-section by adding up contributions from the different C_{60} orbitals. This approach might not be applicable to a cage-like structure such as C_{60}. It could be argued, for instance,

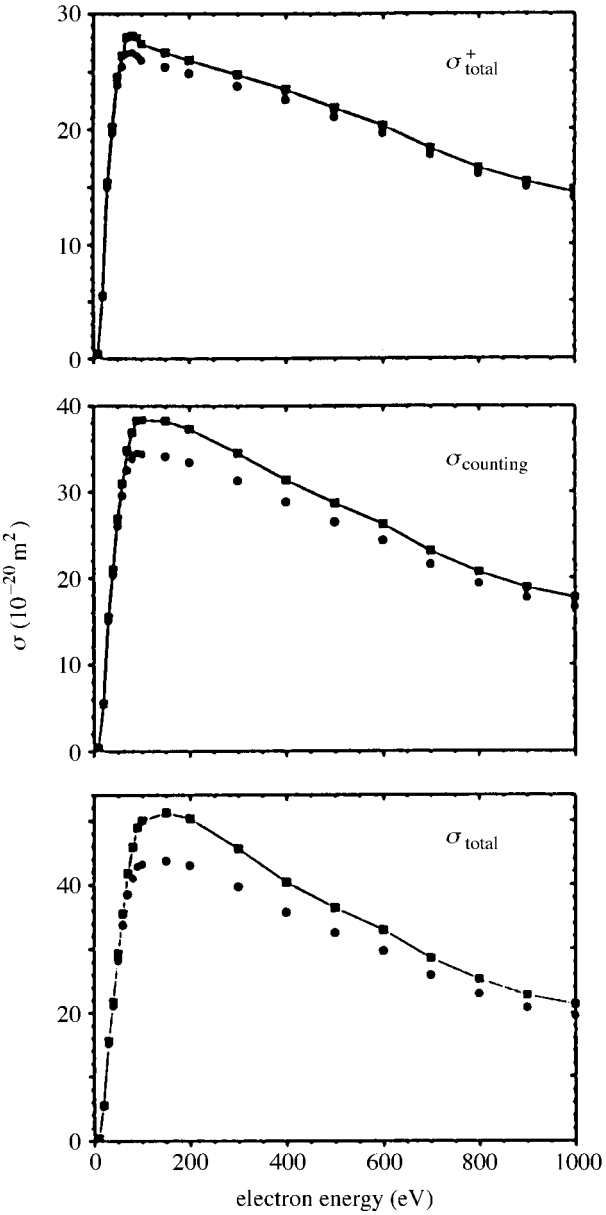

Figure 9. Previously reported (full dots: Matt *et al*. 1996*a*) and corrected (full squares connected by a line to guide the eye (Foltin *et al*. 1998)) values for the C_{60} total single ionization cross-section (σ^+_{total}), counting ionization cross-section (σ_{counting}), and total ionization cross-section (σ_{total}) as a function of electron energy.

that for the incoming projectile only about half of the 60 C atoms that constitute the C_{60} cage are contributing to the cross-sectional area 'seen' by the projectile and that, as a consequence, the calculated cross-sections based on an additivity concept should be multiplied by a factor of 0.5, which would bring them in close agreement

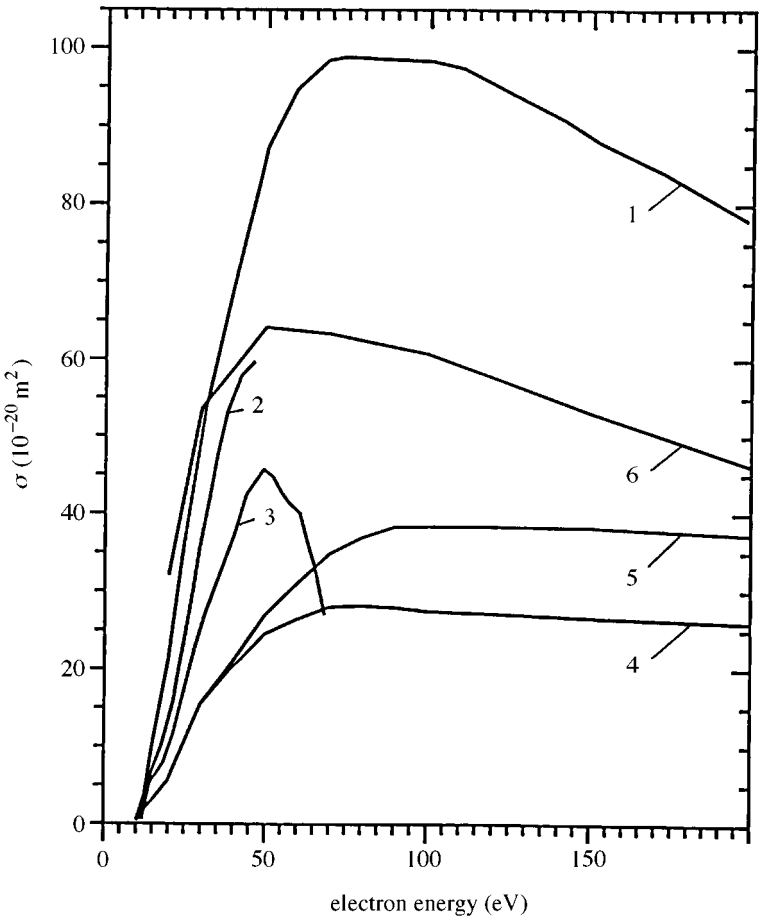

Figure 10. Corrected C_{60} total single ionization cross-sections (curve 4) and counting ionization cross-sections (curve 5) of Matt *et al.* (1996*a*) in comparison with other experimentally determined cross-sections (curve 2, Baba *et al.* (1992*a*); curve 3, Vostrikov *et al.* (1995)) and with calculated cross-sections (curve 1, DM calculation of Deutsch *et al.* (1996); curve 6, modified additivity rule) after Foltin *et al.* (1998).

with the corrected data of Matt *et al.* (1996*a*). As already discussed above, there is poor agreement between the corrected data of Matt *et al.* (1996*a*) (which are in excellent agreement with the very recent data of Tarnovsky *et al.* (1998) and Itoh *et al.* (1999)), and the other two earlier experimental data-sets by Baba *et al.* (1992*a*, *b*) and Vostrikov *et al.* (1995) (curves 2 and 3), both in terms of the cross-section values and in terms of the cross-section shapes.

4. Electron ionization of fullerene ions

A number of collision experiments with fullerene ions has been performed in past years due to the fact that it is fairly simple to produce mass-to-charge selected fullerene ion beams. Salzborn and co-workers, however, were the first to study the interaction of electrons with fullerene ions, and to report interesting and unexpected

cross-section results about electron-impact ionization and fragmentation of singly and multiply charged fullerene ions (Völpel *et al*. 1993; Schäfer *et al*. 1997). Similar studies concerning ionization and dissociation of mass-selected fullerene ions, however, with a specific emphasis on the kinetic energy release in the dissociation reaction, have been recently performed by our group in Innsbruck (Rauth *et al*. 1995; Matt *et al*. 1997*c*). In the following, we will first review the cross-section measurements and then the results concerning the kinetic energy release.

(*a*) *Electron impact ionization cross-sections for fullerene ions*

For the cross-section measurements, Salzborn and co-workers (Völpel *et al*. 1993; Schäfer *et al*. 1997) used their well-established electron–ion crossed-beams technique. The fullerene ions were produced by evaporating carbon soot, containing *ca*. 6% fullerenes, from an oven into the second stage of a 10 GHz electron-cyclotron-resonance (ECR) ion source. Intense ion beams of up to several hundred pA in the case of C_{60}^{+} could be extracted from this source. After acceleration to 7 keV, the ions were momentum analysed using a 90° magnetic sector field (the use of a collimation system in this analysis reduced the ion intensity by more than two orders of magnitude), and crossed at an angle of 90° with an intense electron beam of known current and variable energy. The product ions formed were separated from the primary ion beam and analysed by a second 90° magnetic sector field and detected by a single-particle detector. Simultaneously, the primary ion current was recorded by a Faraday cup. Absolute cross-sections were measured from the respective thresholds up to 1000 eV for single and double ionization and dissociation for various selected primary ions, including C_{60}^{z+} ($z = 1$–3), C_{58}^{+}, C_{70}^{+} and $C_{60,70}^{-}$.

Figure 11 shows, as an example, absolute cross-section functions for single ionization of C_{60}^{z+} ($z = 1$–3) ions and for dissociative single- and double-ionization of C_{60}^{+} to C_{54}^{z+} ($z = 2$–3). Also shown for comparison are the corresponding cross-sections for electron-impact ionization of the neutral C_{60} as reported by Matt *et al*. (1996*a*). Similar to the ionization of the neutral fullerenes there exist different shapes of cross-section functions, depending on the type of the ionization reaction. Moreover, it is interesting to note that a certain correspondence between the ionization of neutrals and the ionization of the corresponding ions can be observed. For instance, the cross-section for single ionization of C_{60} is almost identical (within the combined error bars) in shape and magnitude to that for single ionization of C_{60}^{+}. Nevertheless, in the case of dissociative ionization, the cross-section curves for the ionic targets (though again similar in shape to the corresponding neutral cases) are much larger and are shifted to lower appearance energies. This can be easily understood by taking into account that, to a large extent, the ionic parent target ions will already be highly excited before the interaction with the electron beam. A feature that is especially intriguing, concerning the ionization of fullerene ions, is the reversal of ordering of the magnitude of the single ionization cross-sections for C_{60}^{z+}, e.g. $\sigma(C_{60}^{+} \rightarrow C_{60}^{2+})$ is smaller than $\sigma(C_{60}^{2+} \rightarrow C_{60}^{3+})$, an effect which can also be seen for the C_{58}^{z+} target ion.

(*b*) *Kinetic energy release in electron-induced dissociation of fullerene ions*

In order to study electron-induced ionization and dissociation of mass-selected fullerene ions, we have recently modified the two-sector field mass-spectrometer system, shown in figure 1, in such a way as to allow the study of the inelastic interaction

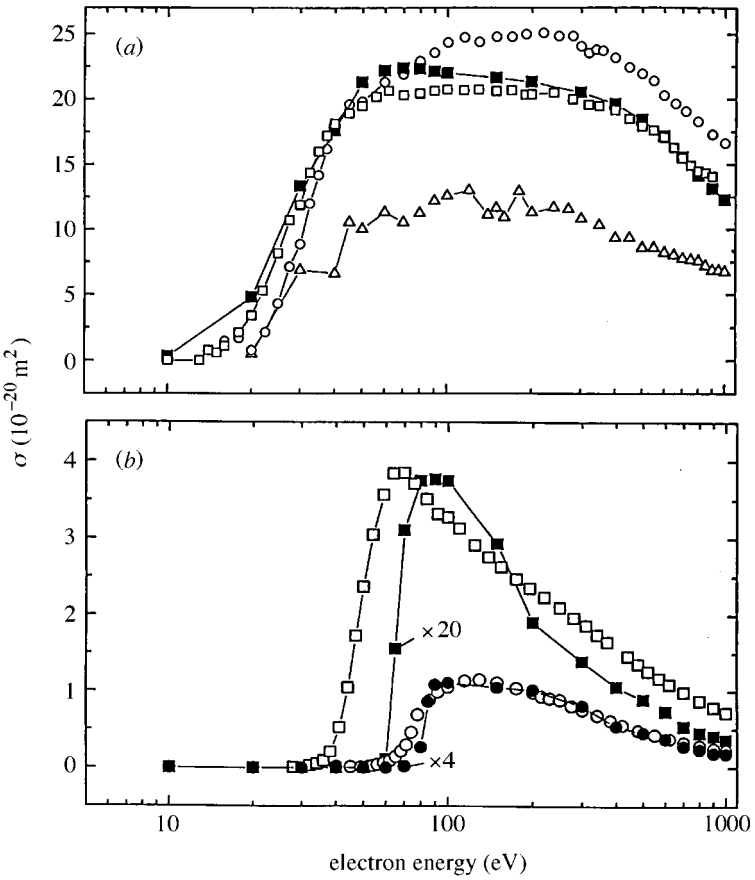

Figure 11. Absolute ionization cross-sections for electron-impact ionization of mass-selected fullerene ions as a function of electron energy (designated by open symbols) after Völpel *et al.* (1993) and Schäfer *et al.* (1997). Also shown for comparison are corresponding cross-sections for electron-impact ionization of neutral C_{60} after Matt *et al.* (1996*a*) designated by the full symbols. (*a*) $C_{60} + e \rightarrow C_{60}^{+}$ (designated by full squares); $C_{60}^{+} + e \rightarrow C_{60}^{2+}$ (designated by open squares); $C_{60}^{2+} + e \rightarrow C_{60}^{3+}$ (designated by open circles); $C_{60}^{3+} + e \rightarrow C_{60}^{4+}$ (designated by open triangles). (*b*) $C_{60} + e \rightarrow C_{54}^{+}$ and $C_{60}^{+} + e \rightarrow C_{54}^{2+}$ (designated by open and full squares, respectively); $C_{60} + e \rightarrow C_{54}^{2+}$ and $C_{60}^{+} + e \rightarrow C_{54}^{3+}$ (designated by open and full circles, respectively). Note that the data in (*b*) designated by full symbols have been multiplied by the factors 20 and 4, respectively, in order to allow a meaningful comparison between the two data-sets.

between electrons and ions in the ion beam focus of the second field-free region, half way between the magnetic and the electrostatic field. Ions passing this second field-free region have already been mass selected by the magnetic sector field. Because ions are produced in this set-up by an ordinary electron-impact ionization Nier-type ion source, the ion currents available, after mass selection, are much lower (i.e. of the order of *ca.* 10 pA) than in the case of an ECR ion source and thus, it was necessary to develop a high-performance electron gun, yielding electron currents beyond 10 mA (Matt *et al.* 1997*c*). With such an electron gun mounted between the two sectors, it was possible to quantitatively investigate electron-induced ionization and

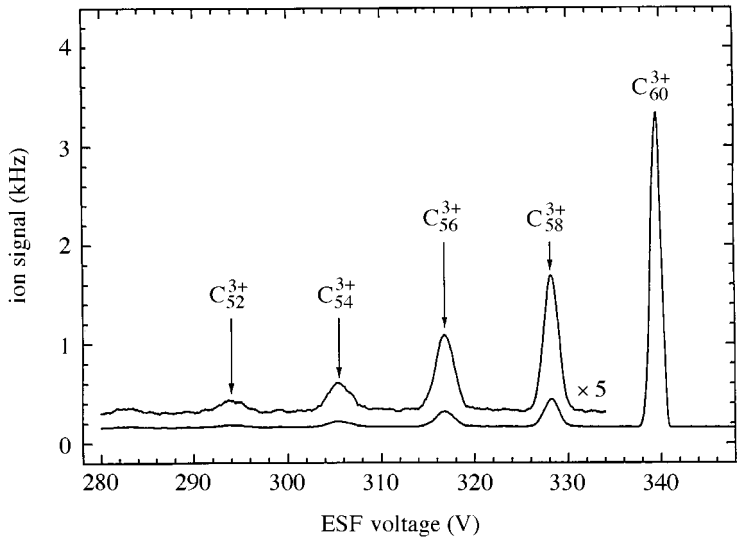

Figure 12. MIKE spectrum (i.e. ion signal versus electric sensor field (ESF) voltage) of triply charged fullerene ions produced by electron ionization of mass-selected doubly charged C_{60}^{2+} ions in the second field-free region of the mass spectrometer shown in figure 1 (after Matt *et al.* 1998*a*, *b*).

fragmentation of mass-selected fullerene ions. In particular, it is possible, by using the MIKE scan technique (see section 2), to identify and analyse fragment ions in terms of their mass and charge state (see figure 12), and to determine the kinetic energy release (see figure 13).

For instance, the position of the respective MIKE peaks (see figure 12), allows an unambiguous identification of the parent and fragment-ion peaks produced by the electron impact. Moreover, from the shape of a MIKE peak it is possible, with help of equation (2.4), to derive the total kinetic energy release distribution (KERD) of a specific decay reaction (see figure 13) after deconvolution of the fragment peak by the respective parent ion peak (see Matt *et al.* (1998*b*, 1999) for more details). In a further step, the mean total kinetic energy release, the $\langle \mathrm{KER} \rangle$ value, of the decay reaction, can be determined by calculating the first moment of the KERD. Figure 13 shows, as an example, the corresponding data (taken with a beta slit of 2 mm width and thus, being slightly broadened due to the influence of this experimental deficiency (see Matt *et al.* 1999)) for C_{58}^{3+} produced by electron-induced ionization and fragmentation of C_{60}^{2+}.

As mentioned in a recent review by Baer & Hase (1996), the determination of the KERD for unimolecular decay of (excited) molecular ions yields valuable information on the energetics and dynamics of the fragmentation reaction. This is even more so if it is possible to measure this property as a function of time, after the formation of the excited ion. For instance, a change in $\langle \mathrm{KER} \rangle$ with increasing lifetime of the excited ion may give valuable information on the transition state, i.e. strongly decreasing $\langle \mathrm{KER} \rangle$ indicating the absence of a reverse activation barrier, and constant or only slightly decreasing $\langle \mathrm{KER} \rangle$ indicating the presence of such a barrier. Complementary information may also be drawn from the peak shape, i.e. flat-topped peaks associated

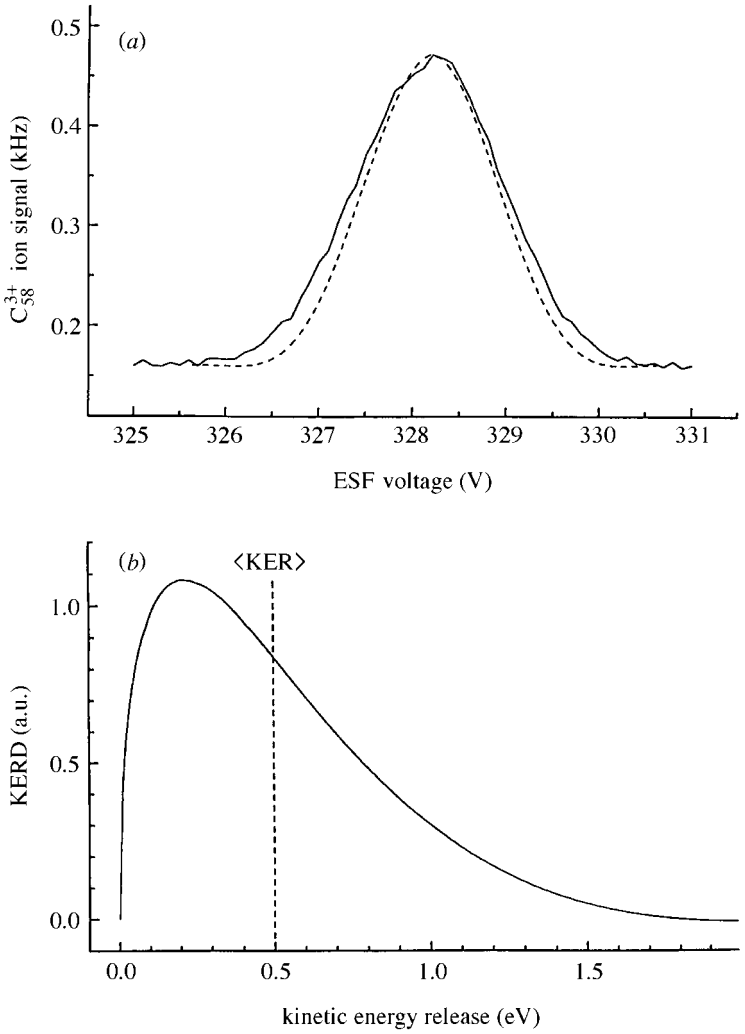

Figure 13. MIKE spectrum (a) of C_{58}^{3+} produced via the electron-impact ionization reaction $C_{60}^{2+} + e \rightarrow C_{58}^{3+} + 2e$ in the second field-free region of the mass spectrometer shown in figure 1 (after Matt *et al*. 1998*a*, *b*). Also shown, the total kinetic energy release distribution KERD (b) derived from this MIKE peak, see text.

with a quasi-single ⟨KER⟩ value are commonly observed for dissociations having appreciable reverse activation barriers (and the large ⟨KER⟩ values are considered to be all, or an appreciable fraction, of the barrier energy) .

One way to measure the KERD, as a function of ion lifetime, is to vary the starting time of the respective sampling time window for the detection of the decay reaction. This can be achieved according to Ji *et al*. (1992) by changing the accelerating voltage of the two-sector field mass spectrometer (for the nominal accelerating voltage of 3 kV, used in the present study, the time-delay between formation of the ion in the ion source and the arrival in the second field-free region is *ca*. 50 μs) or, according

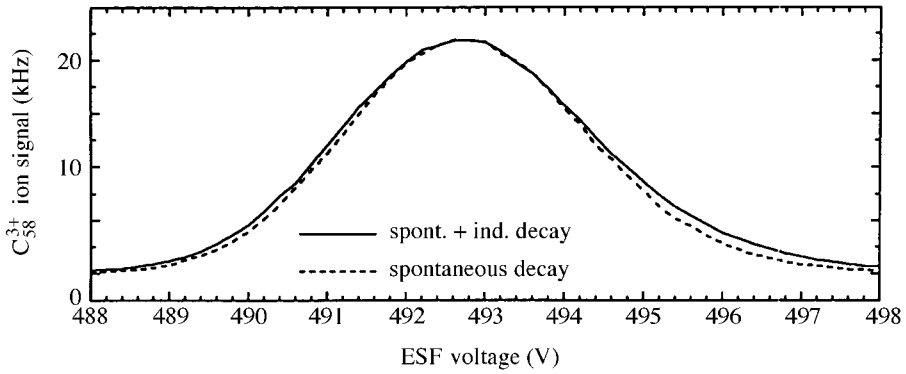

Figure 14. C_{58}^{+} fragment-ion peak (MIKE scan) for the spontaneous decay of the C_{60}^{+} parent ion (designated by dotted line) and for fragment ions produced by both the spontaneous and electron-induced decay of the parent ion (designated by full line) (after Matt *et al*. 1998*b*).

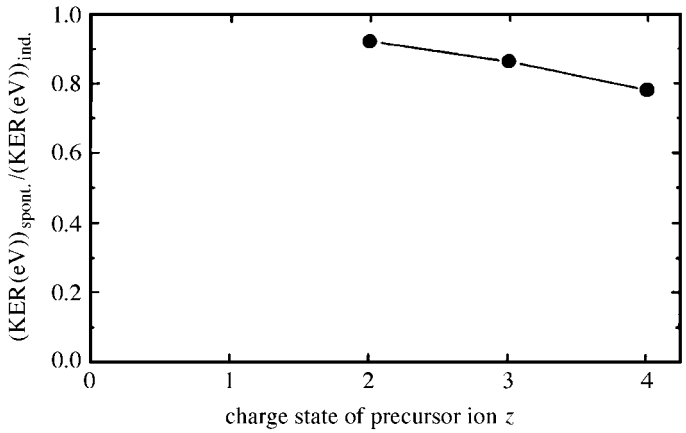

Figure 15. Ratio between ⟨KER⟩ values derived for the spontaneous and the induced decay reactions versus charge state of the decaying C_{60}^{z+} ion (preliminary data after Matt *et al*. 1998*b*).

to Laskin *et al*. (1997), by varying the delay between the ion formation and the ion extraction in an ion trap/reflectron combination. In both cases the KERD is measured for spontaneously decaying ions. Here, we have used a different kind of approach in order to elucidate the time dependence of the kinetic energy distribution of fragment ions, i.e. we investigate, besides the KERD of the spontaneous decay reaction, also the KERD of electron-induced fragmentations of mass-selected ions in the 2ff of the two-sector field mass spectrometer employing the MIKE scan technique thus, giving us the possibility to monitor the decay reaction right after the excitation of the corresponding ion (covering a time window extending from zero up to a few microseconds). Thus, in the case of a decay reaction without reverse barrier (as assumed by several authors when deriving binding energies for C_2 loss from fullerene ions from measured KERD (see Laskin *et al*. 1995)), we expect, for these electron-induced decay reactions, slightly larger kinetic energies.

First measurements for simple electron-induced dissociative excitation reactions,

such as

$$C_{60}^{z+} + e \rightarrow C_{58}^{z+} + C_2 + e \tag{4.1}$$

(where we cannot distinguish, when using the electron excitation of the mass-selected ions, between decay reactions induced by the electron interaction, and spontaneous decay reactions leading to the same fragment ion) clearly show a slight broadening of the fragment-ion peaks in comparison to peaks produced only by spontaneous decay. This indicates the presence of a slightly larger KERD when fragment ions are produced, not only by spontaneous decay reactions but also by electron-induced reactions (see figure 14, giving the KERD for the decay of singly charged C_{60}^{+} ions into C_{58}^{+} fragment ions). As already discussed above, and demonstrated in figure 13, we have measured also the MIKE peaks for reactions

$$C_{60}^{z+} + e \rightarrow C_{58}^{(z+1)+} + C_2 + 2e, \tag{4.2}$$

where a mass-selected precursor ion is ionized into a higher-charge state, and then the decay of this ionized ion is analysed via a MIKE scan of the respective fragment ion. In this case the electron-induced decay reaction is not contaminated by possible spontaneous decay reactions of the mass-selected parent ion, i.e. for the example given in figure 14, C_{60}^{+} into C_{58}^{+}. So far we have investigated electron-induced decays for C_{60}^{z+} ions with z up to 4. In accordance with recent results concerning the singly charged C_{60}^{+} ion by Laskin *et al.* (1997), using an ion trap reflectron mass-spectrometer system, the presently measured and derived preliminary $\langle$KER$\rangle$ values for electron-induced decays are approximately 15% higher than those for spontaneous decays measured under the same experimental conditions concerning the beta slit and the exit slit (see figure 15).

Work supported in part by the FWF, OENB, BMWV, Wien, Austria. It is a pleasure to thank Professor E. Salzborn, Universität Giessen, for providing data before publication.

References

Abrefah, J., Olander, D. R., Balooch, M. & Siekhaus, W. J. 1992 *Appl. Phys. Lett.* **60**, 1313–1314.

Baba, M. S., Narasimhan, T. S. L., Balasubramanian, R. & Mathews, C. K. 1992*a* *Int. J. Mass Spectrom. Ion Proc.* **114**, R1–R8.

Baba, M. S., Narasimhan, T. S. L., Balasubramanian, R. & Mathews, C. K. 1992*b* *Int. J. Mass Spectrom. Ion Proc.* **116**, R1–R6.

Baer, T. & Hase, W. L. 1996 *Unimolecular reaction dynamics, theory and experiments.* Oxford University Press.

Cooks, R., Beynon, J. H., Caprioli, R. M. & Lester, G. R. 1973 *Metastable ions.* Amsterdam: Elsevier.

Deutsch, H., Becker, K., Pittner, J., Bonacic-Koutecky, V., Matt, S. & Märk, T. D. 1996 *J. Phys.* B **29**, 5175–5181.

Dünser, B., Lezius, M., Scheier, P., Deutsch, H. & Märk, T. D. 1995 *Phys. Rev. Lett.* **74**, 3364–3367.

Dünser, B., Echt, O., Scheier, P. & Märk, T. D. 1997 *Phys. Rev. Lett.* **79**, 3861–3864.

Echt, O. & Märk, T. D. 1994 In *Clusters of atoms and molecules II* (ed. H. Haberland). Berlin: Springer.

Foltin, M., Lezius, M., Scheier, P. & Märk, T. D. 1993 *J. Chem. Phys.* **98**, 9624–9634.

Foltin, M., Echt, O., Scheier, P., Dünser, B., Wörgötter, R., Muigg, D., Matt S. & Märk, T. D. 1997 *J. Chem. Phys.* **107**, 6246–6256.

Foltin, V., Foltin, M., Matt, S., Scheier, P., Becker, K., Deutsch, H. & Märk, T. D. 1998 *Chem. Phys. Lett.* **289**, 181–188.

Gong, Q., Sun, Y., Huang, Z., Zhou, X., Gu, Z. & Qiang, D. 1996 *J. Phys.* B **29**, 4981–4986.

Grill, V., Walder, G., Margreiter, D., Rauth, T., Poll, H. U., Scheier, P. & Märk, T. D. 1993 *Z. Phys.* D **25**, 217–226.

Illenberger, E. & Momigny, J. 1992 *Gaseous molecular ions.* Darmstadt: Steinkopff.

Itoh, A., Tsuchida, H., Miyabe, K., Majima, T., Imai, M. & Imanishi, N. 1999 *J. Phys.* B. **32**, 277–286.

Jaffke, T., Illenberger, I., Lezius, M., Matejcik, S., Smith, D. & Märk, T. D. 1994 *Chem. Phys. Lett.* **226**, 213–218.

Ji, Y., Foltin, M., Liao, C. H. & Märk, T. D. 1992 *J. Chem. Phys.* **96**, 3624–3627.

Jin, J., Khemliche, H., Prior, M. H. & Xie, Z. 1996 *Phys. Rev.* A **53**, 615–618.

Klots, C. E. 1985 *J. Chem. Phys.* **83**, 5854–5860.

Klots, C. E. 1990 *Int. J. Mass Spectrom. Ion Proc.* **100**, 457–463.

Kline, L. E., Davies, D. K., Chen, C. L. & Chantry, P. J. 1979 *J. Appl. Phys.* **50**, 6789.

Krätschmer, W., Lamb, L. D., Fostiropolous, K. & Huffman, D. R. 1990 *Nature* **347**, 354.

Kroto, H. W., Heath, J. R., O'Brian, S. C., Curl, R. F. & Smalley, R. E. 1985 *Nature* **318**, 162–163.

Laskin, J. & Lifshitz, C. 1997 *Israel J. Chem.* **37**, 467–474.

Laskin, J., Weikhardt, C. & Lifshitz, C. 1997 *Int. J. Mass Spectrom. Ion Proc.* **161**, L7–L11.

Laskin, J., Jiminez-Vasquez, H. A., Shimshi, R., Saunders, M., deVries, M. S. & Lifshitz, C. 1995 *Chem. Phys. Lett.* **242**, 249–252.

Lifshitz, C. 1993 *Mass Spectrom. Rev.* **12**, 261.

Lezius, M., Scheier, P. & Märk, T. D. 1993 *Chem. Phys. Lett.* **203**, 232–236.

Märk, T. D. 1984 In *Electron–molecule interactions and their applications* (ed. L. G. Christophorou). Orlando: Academic Press.

Märk, T. D. & Dunn, G. H. 1985 *Electron impact ionization.* Wien: Springer.

Margreiter, D., Walder, G., Deutsch, H., Poll, H. U., Winkler, C., Stephan, K. & Märk, T. D. 1990 *Int. J. Mass Spectrom. Ion Proc.* **100**, 143–156.

Matejcik, S., Märk, T. D., Spanel, P., Smith, D., Jaffke, T. & Illenberger, I. 1995 *J. Chem. Phys.* **102**, 2516–2521.

Mathews, C. K., Baba, M. S., Narasimham, T. S. L., Balasubramanian, R., Sivaraman, N., Srinivasan, T. G. & VasudevaRao, P. R. 1992 *J. Phys. Chem.* **96**, 3566.

Matt, S., Dünser, B., Lezius, M., Deutsch, H., Becker, K., Stamatovic, A., Scheier P. & Märk, T. D. 1996*a* *J. Chem. Phys.* **105**, 1880–1896.

Matt, S., Muigg, D., Ding, A., Lifshitz, C., Scheier, P. & Märk, T. D. 1996*b* *J. Phys. Chem.* **100**, 8692–8696.

Matt, S., Echt, O., Wörgötter, R., Grill, V., Scheier, P., Lifshitz, C. & Märk, T. D. 1997*a* *Chem. Phys. Lett.* **264**, 149–156.

Matt, S., Echt, O., Wörgötter, R., Scheier, P., Klots, C. E. & Märk, T. D. 1997*b* *Int. J. Mass Spectrom. Ion Proc.* **167/168**, 753–759.

Matt, S., Echt, O., Rauth, T., Dünser, B., Lezius, M., Stamatovic, A., Scheier, P. & Märk, T. D. 1997*c* *Z. Phys.* D **40**, 389–394.

Matt, S., Scheier, P., Märk, T. D. & Becker, K. 1998*a* In *Novel aspects of electron–molecule collisions* (ed. K. Becker). Singapore: World Scientific Publishing.

Matt, S., Sonderegger, M., David, R., Fiegele, T., Mair, C., Biasioli, F., Stamatovic, A., Scheier, P. & Märk, T. D. 1998*b* In *Book of Invited Lectures: 11th Symp. on Elementary Processes and Chemical Reactions in Low Temperature Plasmas*, Slovak Republic.

Matt, S., Sonderegger, M., Rainer, D., Echt, O., Scheier, P., Laskin, J., Lifshitz, C. & Märk, T. D. 1999 *Int. J. Mass Spectrom. Ion Proc.* (In the press.)

Rauth, T., Echt, O., Scheier, P. & Märk, T. D. 1995 *Chem. Phys. Lett.* **247**, 515–521.

Schäfer, V., Hathramani, D., Aichele, K., Hartenfelle, U., Scheuermann, F. & Salzborn, E. 1997 In *Book of Abstracts of XXth ICPEAC* (ed. F. Aumayr, G. Betz & H. P. Winter). Wien: Institut für Allgemeine Physik, Technische Universität Wien.

Scheier, P. & Märk, T. D. 1994 *Phys. Rev. Lett.* **73**, 54–57.

Scheier, P. & Märk, T. D. 1997 *Mitteilungsblatt Österr. Phys. Gesellschaft* **1**, 11.

Scheier, P., Dünser, B. & Märk, T. D. 1995 *Phys. Rev. Lett.* **74**, 3368–3371.

Scheier, P., Dünser, B., Wörgötter, R., Muigg, D., Matt, S., Echt, O., Foltin, M. & Märk, T. D. 1996*a* *Phys. Rev. Lett.* **77**, 2654–2657.

Scheier, P., Dünser, B., Wörgötter, R., Matt, S., Muigg, D., Senn, G. & Märk, T. D. 1996*b* *Int. Rev. Phys. Chem.* **15**, 93–131.

Schmalz, T. G., Seitz, W. A., Klein, D. J. & Hite, G. E. 1988 *J. Am. Chem. Soc.* **110**, 1113–1127.

Schwarz, H. 1993 *Nova Acta Leopoldina* **69**, 167–181.

Smith, A. L. 1996 *J. Phys.* B **29**, 4975–4980.

Smith, D., Spanel, P. & Märk, T. D. 1993 *Chem. Phys. Lett.* **213**, 202–206.

Tarnovsky, V. & Becker, K. 1993 *J. Chem. Phys.* **98**, 7868–7874.

Tarnovsky, V., Kurunczi, P., Matt, S., Märk, T. D., Deutsch, H. & Becker, K. 1998 *J. Phys.* B **31**, 3043–3048.

Völpel, R., Hofmann, G., Steidl, M., Stenke, M., Schlapp, M., Trassl, R. & Salzborn, E. 1993 *Phys. Rev. Lett.* **71**, 3439–3442.

Vostrikov, A. A., Dubov, D. Y. & Agarkov, A. A. 1995 *Tech. Phys. Lett.* **21**, 715–716.

Wennerström, O., Lindqvist, K. & Barany, A. 1996 The Nobel Prize in Chemistry. *The Royal Swedish Academy of Sciences*. Stockholm: Tryckindustri.

Wörgötter, R., Dünser, B., Scheier, P. & Märk, T. D. 1994 *J. Chem. Phys.* **101**, 8674–8679.

Wörgötter, R., Dünser, B., Scheier, P., Märk, T. D., Foltin, M., Klots, C. E., Laskin, J. & Lifshitz, C. 1996 *J. Chem. Phys.* **104**, 1225–1231.

Yannouleas, C. & Landman, U. 1994 *Chem. Phys. Lett.* **252**, 277.

PHILOSOPHICAL TRANSACTIONS OF THE ROYAL SOCIETY A MATHEMATICAL, PHYSICAL & ENGINEERING SCIENCES

PHILOSOPHICAL TRANSACTIONS OF THE ROYAL SOCIETY A MATHEMATICAL, PHYSICAL & ENGINEERING SCIENCES